Isotope shift in the sulfur electron affinity: Observation and theory

Thomas Carette,[1] Cyril Drag,[2] Oliver Scharf,[1] Christophe Blondel,[2] Christian Delsart,[2]
Charlotte Froese Fischer,[3] and Michel Godefroid[1,*]

[1]*Chimie Quantique et Photophysique, Université Libre de Bruxelles - CP160/09, B-1050 Brussels, Belgium*
[2]*Laboratoire Aimé-Cotton, CNRS, Université Paris-sud, F-91405 Orsay cedex, France*
[3]*National Institute of Standards and Technology Gaithersburg, Maryland 20899-8420, USA*

(Received 5 February 2010; published 28 April 2010)

The sulfur electron affinities ${}^eA(\mathrm{S})$ are measured by photodetachment microscopy for the two isotopes ^{32}S and ^{34}S (16 752.975 3(41) and 16 752.977 6(85) cm^{-1}, respectively). The isotope shift in the electron affinity is found to be more probably positive, ${}^eA(^{34}\mathrm{S}) - {}^eA(^{32}\mathrm{S}) = +0.0023(70)$ cm^{-1}, but the uncertainty allows for the possibility that it may be either "normal" [${}^eA(^{34}\mathrm{S}) > {}^eA(^{32}\mathrm{S})$] or "anomalous" [${}^eA(^{34}\mathrm{S}) < {}^eA(^{32}\mathrm{S})$]. The isotope shift is estimated theoretically using elaborate correlation models, monitoring the electron affinity and the mass polarization term expectation value. The theoretical analysis predicts a very large specific mass shift (SMS) that counterbalances the normal mass shift (NMS) and produces an anomalous isotope shift ${}^eA(^{34}\mathrm{S}) - {}^eA(^{32}\mathrm{S}) = -0.0053(24)$ cm^{-1}, field shift corrections included. The total isotope shift can always be written as the sum of the NMS (here $+0.0169$ cm^{-1}) and a residual isotope shift (RIS). Since the NMS has nearly no uncertainty, the comparison between experimental and theoretical RIS is more fair. With respective values of $-0.0146(70)$ cm^{-1} and $-0.0222(24)$ cm^{-1}, these residual isotope shifts are found to agree within the estimated uncertainties.

DOI: 10.1103/PhysRevA.81.042522 PACS number(s): 31.30.Gs, 31.15.ve, 32.80.Gc, 32.10.Hq

I. INTRODUCTION

Photodetachment microscopy, which is the analysis of the electron interference pattern naturally produced when photodetachment occurs in the presence of an electric field [1,2], was applied to a beam of $^{32}S^-$ ions and allowed to measure the detachment thresholds corresponding to different fine-structure levels of the negative ion S^- and the neutral atom S [3]. The electron affinity of sulfur, at 2.077 eV, is well suited for detachment by a tunable dye laser, which provides a third way of measuring neutral S fine structure, besides VUV spectroscopy of S I lines and direct fine-structure resonance spectroscopy. Dye laser photodetachment of S^- was also used as a probe of microwave-induced transitions of hyperfine-split Zeeman transitions, which lead to a measurement of the hyperfine structure of $^{33}S^-$ [4]. The fine structures of S^- and neutral S, with the definition of the six "fine-structure detachment thresholds," labeled A, B, C, D, E, and F (in the order of increasing excitation energy) are displayed in Fig. 1. In the present work, photodetachment microscopy is used to measure the electron affinity ${}^eA$ (threshold C) of the even isotopes 32 and 34 of sulfur. The sensitivity of the method made it possible to record a significant number of ^{34}S detachment events, even though sulfur was produced from a chemical compound with no isotopic enrichment and detachment occurred at very low energies above threshold (namely in the sub-meV range). The accuracy of photodetachment-microscopy-based electron affinity measurements makes it possible to get an estimate of the isotope shift, precise enough to make comparison with theory significant.

On the theoretical side, the *ab initio* calculation of electron affinities is a challenge. Various methods for evaluating electron binding energies and affinities are discussed by Lindgren [5], presenting five different techniques, from the Koopmans-theorem method, up to the density-functional theory. Lindgren's survey focuses on the many-body perturbation approach and only mentions, without further discussion, a sixth method that can always be used: separate many-body calculations for the initial and final states, using some elaborate variational technique, like multiconfiguration or configuration-interaction methods. This approach can indeed be successful for small systems (see for instance Ref. [6] for ^{7}Li) and is precisely the one attempted in the present work, although the correlation balance is more difficult to achieve for a large number of electrons.

The electron affinity of sulfur has been estimated, after the pioneering work of Clementi *et al.* [7], by Woon and Dunning [8] who treated the second row atoms through multireference single and double excitation configuration-interaction calculations and by Gutsev *et al.* [9] using the coupled-cluster method. In a benchmark study of *ab initio* and density-functional calculations of electron affinities covering the first- and second-row atoms, de Oliveira *et al.* [10] concluded that the best *ab initio* results agree, on average, to better than 0.001 eV with the most recent experimental results. For heavy systems, the relativistic effects become crucial [11,12] and an accuracy better than 0.04 eV (10%) was difficult to achieve for the electron affinity of lead in the full relativistic approach [13].

The search for a possible variation of the fine-structure constant α has renewed interest in developing reliable *ab initio* computational methods for atomic spectra [14,15]. Theory versus experiment comparisons of atomic isotope shifts can serve as sensitive tests of our computational ability for some important electronic factors. Stimulated by photodetachment experiments [16,17], theoretical calculations on isotope shifts in electron affinities have been attempted for oxygen [18,19], using the numerical multi-configuration Hartree-Fock (MCHF) approach. Beryllium was another interesting target [20], but *ab initio* calculations remain scarce, requiring the calculation of two properties—the electron affinity *and* its isotope

*mrgodef@ulb.ac.be

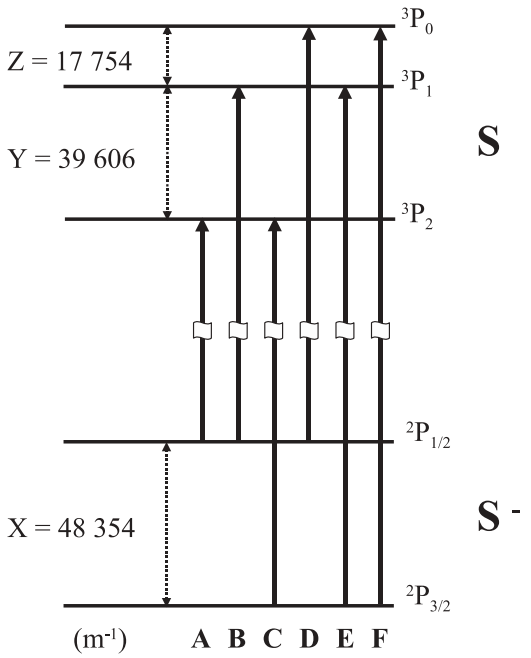

FIG. 1. S^- fine-structure detachment thresholds. Energies measured with wavenumbers in m^{-1} (figure taken from [3]).

shift—both highly sensitive to correlation effects. For these systems, the limited population and the restricted active space concepts were used to build the configuration spaces. Adopting similar correlation models for the S/S^- system becomes prohibitive and efficient reduction strategies need to be found.

In the present work, various single- and double-multireference valence expansions sets are explored for a full nonrelativistic variational optimization of the wave function through the MCHF procedure. Core excitations from these multireference sets are included afterward through configuration-interaction. Computational strategies are investigated and developed by monitoring the electron affinity and the mass polarization expectation values difference between the neutral atom and the negative ion.

The experimental work and theoretical calculations are presented in Secs. II and III, respectively. The comparison of observation and theory is discussed in Sec. IV.

II. EXPERIMENTAL MEASUREMENT OF THE ISOTOPE SHIFT

A. Experimental setup

1. Ion beam and isotope selection

Photodetachment microscopy was performed on a beam of S^- produced by a hot cathode discharge in a mixture of 98% Ar and 2% CS_2. This commercial mixture had no isotopic enrichment, so the isotopes of sulfur were produced with their natural abundance, which meant only 4% [21] of $^{34}S^-$ (i.e., only a few pA). With such a barely measurable ion current, all the electrostatic settings of the ion beam and the alignment of the laser in the interaction region had to be done with our Wien velocity filter set on mass 32. Then the electric field applied in the Wien filter was reduced by the factor $4/\sqrt{17}$ appropriate for shifting from mass 32 to mass 34. We checked that the electron interferograms obtained with this setting were not a residue of the $^{32}S^-$ signal on the wing of the maximum of mass-32 transmittance. A primary observation was that the peaks of the mass spectrum, when recorded on the total ion current signal (including a very visible contribution of SH^- at mass 33) appeared well separated, which meant a mass resolution of 70 at least. A more quantitative limit of the possible admixture of the 32 signal at mass 34 was given by setting the velocity filter at mass 33, and observing that this actually let no photoelectron signal emerge from the background of the electron image, even though we recorded the impacts on the detector for a time longer than the one needed to reconstruct visible interference rings at mass 34. One mass unit away from its maximum, the $^{32}S^-$ current was thus much lower than the $^{34}S^-$ maximum current. Since isotope 32 is 22 times more abundant than isotope 34, this means a factor of attenuation of 100 at least. Two units away from the 32 maximum, the attenuation must be even more complete, so the few $^{32}S^-$ detachment events remaining at mass 34 are certainly negligible with respect to the electron background due to parasitic collisions of the ion beam with the diaphragms or the residual gas and to the 34 signal itself.

2. Laser photodetachment

As in previous photodetachment microscopy experiments on sulfur [3,22], laser excitation was provided by a CW ring dye laser (Spectra-Physics 380A [23]) operating with Rhodamine 590 in 5% methanol and 95% ethylene-glycol. Single-mode operation was achieved by means of a pair of intracavity Fabry-Perot etalons. The cavity length is servo-locked by means of an external sigmameter [24]. Thanks to stabilization of the sigmameter itself on the wavelength of a dual-polarization stabilized He-Ne laser, the frequency of the tunable laser can remain stable within a few MHz for the typically 20 minutes needed to record every photoelectron interferogram. The wavenumber of the laser is measured by an Ångstrom WS-U lambdameter, with an accuracy better than 10^{-3} cm^{-1}.

B. Experimental data

1. Photodetachment interferograms

Figure 2 gives an example of a pair of interferograms obtained from a double pass of the laser beam on the ion beam. This double pass makes it possible to obtain Doppler-free measurements, by averaging the responses of both spots, for they correspond to symmetric residual deviations from 90° of the laser-ion intersection angle (cf. [25]). Due to the rarity of ^{34}S, even after an accumulation time of 2000 s, the number of electrons counted per pixel is eight at its maximum. Nevertheless, this is enough for the fitting program to find the center and contour of each spot, and to calculate a histogram of the average number of electrons counted per pixel at a given distance from the center. The obtained radial profile, as shown on Fig. 3, gives a much less noisy picture of the interference pattern and shows its excellent correspondence with theory [even though the actual fitting procedure is done on the two-dimensional (2D) electron distribution]. The phase (i.e., 2π times the number of oscillations in the interferogram) is the essential parameter for determining the initial kinetic energy of the electron. The interferometric accuracy so obtained, of

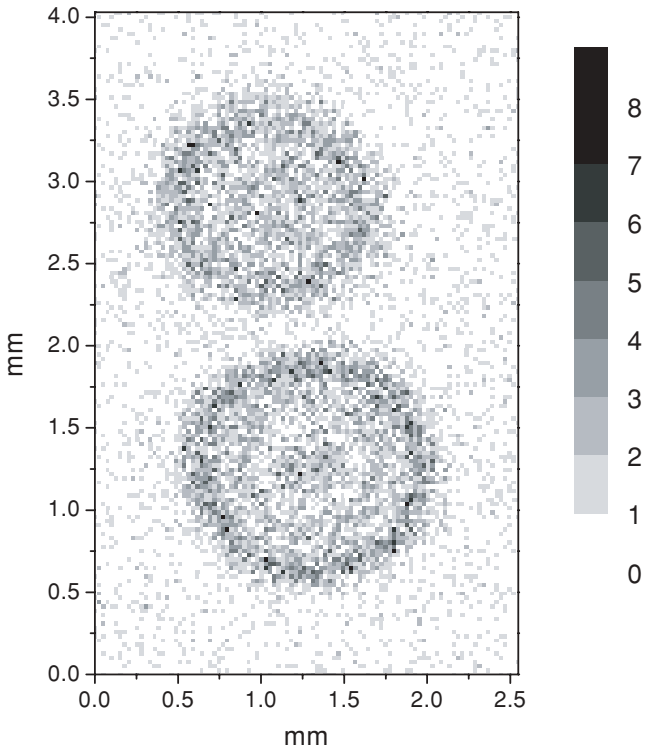

FIG. 2. Double interferogram obtained from $^{34}S^-$ at a wavelength $\lambda = 596.89056(2)$ nm, in an electric field 291 V/m, for an accumulation time of 2000 s. The grey scale indicates the total number of electrons counted in each pixel. The data are recorded by means of a Quantar Technology Inc. particle detector of the series 3391 with the 2251 Image-Trak™ enhanced software. The presented image was reprocessed with Microcal™ Origin®.

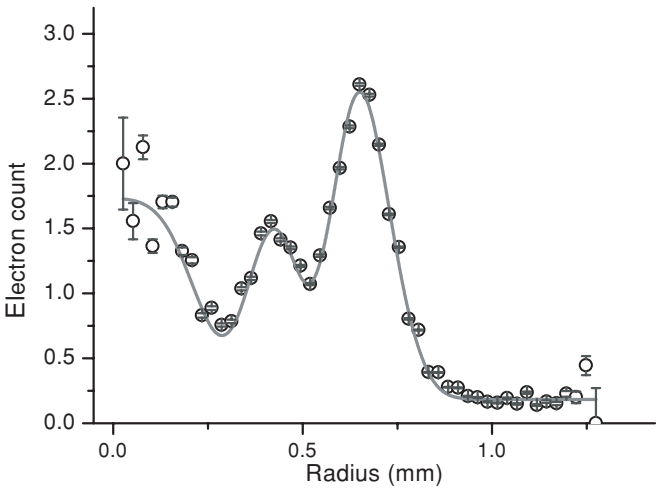

FIG. 3. Average number of electrons counted per pixel, in the lower spot of Fig. 2. The continuous line is the radial profile calculated with the best-fitting parameters (as provided by an adjustment algorithm applied to the original 2D data). One among these parameters is the initial kinetic energy of the electron, here found to be 0.5819(37) cm^{-1} (but the 1σ error bar given here assumes no uncertainty at all on the electric field itself).

the order of a few 10^{-3} cm^{-1}, is orders of magnitude better than what a measurement of the spot diameter would provide. The latter would actually pertain to the domain of classical electron spectrometry, the accuracy of which is seldom better than 1 meV, or a few cm^{-1}.

2. *Data analysis*

In principle, photodetachment microscopy does not require a series of photodetachment images to be recorded to get a measure of the electron affinity ${}^eA$. Calculating the difference between the photon energy and the measured electron kinetic energy in a single experiment will give the result. However, any discrepancy between the expected and actual values of the electric field in the photodetachment region is able to produce a systematic shift of the measured photoelectron energies. This being a constant relative error, extrapolating the measured electron affinity down to zero initial kinetic energy (i.e., to the detachment threshold) provides a method for avoiding the electric-field uncertainty [22,26]. A series of measured electron affinities obtained both for isotope 32 and isotope 34 are represented in Fig. 4.

Extrapolation of the measured ${}^eA$ values down to zero being the leading idea, we had to admit that the few experimental points obtained would not be enough to determine the slope of the linear regression, for the ^{34}S case, with a satisfying accuracy. The idea was thus to make ^{32}S and ^{34}S measurements in similar experimental conditions, and make the linear regression with a constraint of similarity on the slopes, to set the ^{34}S slope with improved accuracy. The experimental data shown in Fig. 4 for ^{32}S were actually taken during the same runs as the ^{34}S ones. The difference between the ^{34}S and ^{32}S slopes may thus be constrained by a normal distribution with a characteristic width of 0.5%, which is an estimate (on the larger side) of the typical slope variations observed in past experiments done in similar conditions. As a matter of fact, fitting the data with this constraint yields nearly identical slopes of 0.18% and 0.16% for ^{32}S and ^{34}S, respectively, the

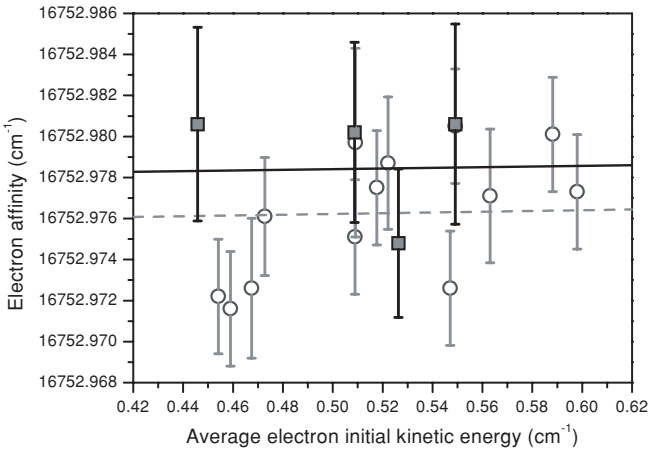

FIG. 4. Comparison of electron affinity measurements made in common series of experiments for ^{32}S (circles) and ^{34}S (squares), with the average trend for each isotope (dashed line is 32, continuous line is 34), assuming similar dependencies of the apparent electron affinity as a function of the average electron kinetic energy. The data shown in Fig. 2 produce the experimental ^{34}S point at 0.509 cm^{-1}.

visual consequence of this result being that the two regression lines drawn in Fig. 4 appear nearly parallel.

3. Experimental results

The electron affinities ${}^eA(\mathrm{S})$, which are the ordinates at zero energy of the two lines drawn on Fig. 4, are 16 752.975 3(41) and 16 752.977 6(85) cm^{-1} for ^{32}S and ^{34}S, respectively. The error bars given here take the statistical distribution of the data into account at a 2σ level together with a possible $\pm 10^{-3}$ cm^{-1} systematic error on wavenumber measurements. The value of ${}^eA(^{32}\mathrm{S})$ incorporates all our previous work that led to the published result of 16 752.976 0(42) cm^{-1} [3]. The subsequent discovery that transverse magnetic-field effects were actually negligible [27] was applied to these former data, but accounts only for -0.0001 of the -0.0007 revision of the most probable value of ${}^eA(^{32}\mathrm{S})$ down to 16 752.975 3(41) cm^{-1}; ${}^eA(^{32}\mathrm{S})$ remains the most accurately known of all electron affinities.

The isotope shift ${}^eA(^{34}\mathrm{S})$-${}^eA(^{32}\mathrm{S})$ is found to be $+0.0023(70)$ cm^{-1}. Having a better accuracy on the difference than on the least well known of both electron affinities is a logical consequence of the experimental method. The direct comparison of the apparent electron affinities at similar detachment energies naturally provides a good accuracy on the isotope shift, even though the linear regression to the actual value of ${}^eA$ suffers from additional experimental unknowns. The strong covariance of the electron affinities is reinforced by the inclusion of the possible systematic error on wavelength measurements, which is, by definition, the same in both cases. Numerically, the final correlation found between the obtained variances of the electron affinities is $+0.57$.

III. THEORY AND *AB INITIO* CALCULATIONS

A. Theoretical isotope shift

Adopting the $(A' > A)$ convention where A is the mass number, the isotope shift on the electron affinity defined as

$$IS(A', A) = \delta\, {}^eA \equiv {}^eA(A') - {}^eA(A), \tag{1}$$

is expressed as the sum of the normal mass shift (NMS), specific mass shift (SMS), and field shift (FS) contributions

$$IS(A', A) = \delta^e A_{\mathrm{NMS}} + \delta^e A_{\mathrm{SMS}} + \delta^e A_{\mathrm{FS}}. \tag{2}$$

Introducing M for the nuclear mass and X for the chemical element, the two first terms that constitute the mass shift can be written in atomic units ($m_e = 1$ and $\hbar = 1$) as

$$\delta^e A_{\mathrm{NMS}} + \delta^e A_{\mathrm{SMS}} = \left[\frac{M'}{1+M'} - \frac{M}{1+M}\right] {}^eA(\infty) + \left[\frac{M'}{(1+M')^2} - \frac{M}{(1+M)^2}\right] \Delta S_{\mathrm{SMS}}, \tag{3}$$

where

$$\Delta S_{\mathrm{SMS}} = S_{\mathrm{SMS}}(X) - S_{\mathrm{SMS}}(X^-), \tag{4}$$

with

$$S_{\mathrm{SMS}} = -\langle \Psi_\infty | \sum_{i<j}^{N} \nabla_i \cdot \nabla_j | \Psi_\infty \rangle. \tag{5}$$

This expression is correct to first order in μ/M, where $\mu = m_e M/(m_e + M)$ is the reduced mass of the electron with respect to the nucleus. For a positive ΔS_{SMS} difference, the NMS and SMS interfere negatively due to the relative signs of the mass factors in Eq. (3) [20]. It is easy to show that the degree of cancellation between NMS and SMS is basically governed by the mass-independent difference $[{}^eA(\infty) - \frac{\hbar^2}{m_e}\Delta S_{\mathrm{SMS}}]$. The two atomic masses of ^{32}S (31.972 071 00 u) and ^{34}S (33.967 866 90 u), taken from the AME2003 compilation of Audi *et al.* [28] are converted into nuclear masses by subtracting the electron mass contribution (0.027%) [29].

The FS can be estimated from

$$\delta^e A_{\mathrm{FS}} = (hc) 4\pi \left[\rho(\mathbf{0})^X_{NR} - \rho(\mathbf{0})^{X^-}_{NR}\right] \frac{a_0^3}{4Z} f(Z)^{AA'} \times [\langle r^2\rangle_{A'} - \langle r^2\rangle_A], \tag{6}$$

where $\rho(\mathbf{0})_{NR}$ is the nonrelativistic spin-less total electron density $\rho(\mathbf{r})$ (in a_0^{-3}) calculated at $\mathbf{r} = \mathbf{0}$ [30]. The factor $f(Z)^{32-34} = 0.014\,823$ $\mathrm{cm}^{-1}/\mathrm{fm}^2$ is taken from Aufmuth *et al.* [31] and corrects for the fact that we use the nonrelativistic electronic density for a point nucleus. The $\langle r^2\rangle^{1/2}_{32} = 3.2608(18)$ fm and $\langle r^2\rangle^{1/2}_{34} = 3.2845(21)$ fm values are taken from Angeli [32].

Note from Eq. (6) that with a positive variation of the rms nuclear charge radii (i.e., $\delta\langle r^2\rangle^{AA'} \equiv \langle r^2\rangle_{A'} - \langle r^2\rangle_A \geqslant 0$) the FS has the same sign as the NMS if and only if the electron detachment ($X^- \rightarrow X$) is accompanied by an increase of the electron density at the nucleus ($\Delta\rho(\mathbf{0}) \geqslant 0$). For a system like sulfur, the FS is expected to be much smaller than the mass shift. Therefore, our computational strategy is dictated by the description of the electron affinity and ΔS_{SMS}, although the FS is taken into account in the present analysis (see Sec. IV).

B. Computational method

We use the numerical MCHF approach describing the atomic wave function as

$$\Psi = \sum_i c_i \Phi(\gamma_i LS), \tag{7}$$

where $\{\Phi(\gamma_i LS)\}$ is an orthonormal set of configuration state functions (CSF) that are symmetry adapted linear combinations of Slater determinants [33,34]. In this method, the radial functions $\{P_{nl}(r)\}$ defining the orbital active set and the mixing coefficients $\{c_i\}$ are variational. The configuration-interaction (CI) method solves the eigenvalue problem in a CSF basis built with a fixed preoptimized orbital set.

For any differential property that is estimated from the difference between two calculated diagonal properties using the variational approach, much care must be taken to obtain a good balance between the two states. It becomes even more difficult when the latter belong to systems with different numbers of electrons. In such situations, the ATSP2K package [35] is an efficient tool thanks to its flexibility. In particular, the fully implemented *limited population* (LP) and *multi-reference* (MR) [36,37] approaches for building the configuration space offer systematic ways of including and monitoring correlation. While the LP configuration space is built by allowing single (S)-, double (D)-, triple (T)-, and possibly higher excitations, from a single reference configuration state

function, restricted by orbital occupation, the MR method is usually limited to SD excitations from a larger set of configuration states. The LP method has been successfully used to calculate the isotope shifts in the oxygen electron affinity [18,19]. Although both the LP and MR correlation models have been explored, the present theoretical discussion is limited to the multireference calculations.

C. The experimental electron affinity as a guideline

In our approach, the experimental electron affinity is used as a guideline to set efficient pathways in the variational configuration spaces. Our nonrelativistic approach targets electron correlation. In this context, it is useful to get a reference nonrelativistic ${}^eA$ value. Introducing the observed average energy levels

$$\overline{E} = \frac{\sum_J (2J+1)E_J}{\sum_J (2J+1)}, \tag{8}$$

for both S $3p^4\ {}^3P$ and $S^-\ 3p^5\ {}^2P^o$, the average experimental electron affinity that would be measured if not resolving the fine-structure thresholds, is estimated from

$$\begin{aligned} {}^eA^{\rm AV}_{\rm exp} &= \overline{E}(S\ {}^3P) - \overline{E}(S^-\ {}^2P^\circ) \\ &= \frac{(E_0 + 3E_1 + 5E_2)}{9} - \frac{(2E_{1/2} + 4E_{3/2})}{6}. \end{aligned} \tag{9}$$

This average energy can be rewritten in terms of some deviation to the observed electron affinity ${}^eA_{\rm exp} = (E_2 - E_{3/2})$ (arrow C in Fig. 1)

$${}^eA^{\rm AV}_{\rm exp} = {}^eA_{\rm exp} + \frac{3(E_1 - E_2) + (E_0 - E_2)}{9} - \frac{(E_{1/2} - E_{3/2})}{3}. \tag{10}$$

Using ${}^eA_{\rm exp} = 16\,752.975\,3(41)\ {\rm cm}^{-1}$ reported in Sec. II B3 for ${}^{32}S$ and the observed fine structures of S and S^- [3], the Sulfur average experimental electron affinity ${}^eA^{\rm AV}_{\rm exp} = 16\,787.55\ {\rm cm}^{-1} = 2.081\,391\ {\rm eV} = 0.076\,489\,702\ {\rm E_h}$ is obtained from Eq. (10).

When adopting a Breit-Pauli description [34,38] of atomic structures, the total binding energy $E(LSJ)$ of a level is expressed in first-order perturbation theory as

$$E(LSJ) = E^{\rm NR}_{LS} + E^{\rm NF}_{LS} + E^{\rm F}_{LSJ}, \tag{11}$$

that is, as the summation of the nonrelativistic total energy ($E^{\rm NR}$), the non-fine-structure relativistic shift ($E^{\rm NF}$) and the J-dependent fine-structure correction ($E^{\rm F}$). Since the fine structures of both S $3p^4\ {}^3P$ and $S^-\ 3p^5\ {}^2P^o$ are washed out by the averaging process (10) to get ${}^eA^{\rm AV}_{\rm exp}$, a reference nonrelativistic electron-affinity ${}^eA^{\rm NR}_{\rm ref}$ is estimated by subtracting the corresponding theoretical non-fine-structure contribution $\Delta E^{\rm NF} = E^{\rm NF}(S) - E^{\rm NF}(S^-)$, from the above experimental average electron affinity

$${}^eA^{\rm NR}_{\rm ref} = {}^eA^{\rm AV}_{\rm exp} - \Delta E^{\rm NF}. \tag{12}$$

The non-fine-structure contribution calculated in the single configuration Hartree-Fock approximation, $\Delta E^{\rm NF}_{\rm HF} = -5.362\,51\ 10^{-4}\ {\rm E_h}$, produces a nonrelativistic electron-affinity value of ${}^eA^{\rm NR}_{\rm ref} = 0.077\,026\ {\rm E_h}$. Note that the latter value is in line with the estimation of the "nonrelativistic experimental" electron-affinity ($0.076\,939\ {\rm E_h}$) calculated from the scalar contribution of de Oliveira *et al.* [10], who found an excellent general agreement for electron affinities of first- and second-row atoms.

D. The multireference approach

1. MR-MCHF calculations

In the multireference approach, one first defines a zeroth-order set of CSF's labeled MR

$${\rm MR} \equiv \{\Phi_1(\gamma_1 LS\pi), \Phi_2(\gamma_2 LS\pi), \ldots, \Phi_m(\gamma_m LS\pi)\}, \tag{13}$$

that includes the dominant interacting terms in the description of a given atomic state. This zeroth-order set is then expanded to capture major correlation effects. Useful expansions are built by allowing all single and double excitations from a multireference (MR-SD) set within a given orbital active space. From a practical point of view, these expansions are generated using LSGEN [39] that produces the desired list of configurations, containing the complete set of CSF's for a given $LS\pi$-total symmetry.

A good valence correlation MR-SD expansion for S^- is based on the multireference set

$${\rm MR}(S^-) = \{1,2\}^{10}\{3s,3p\}^5\{3,4\}^2. \tag{14}$$

The notation is inspired from the LP approach: the multireference set (14) is composed of all CSF's having the required symmetry (here ${}^2P^o$), with ten electrons $\{1,2\}^{10}$ forced to occupy the $n=1$ and $n=2$ shells (i.e., a $1s^2 2s^2 2p^6$ closed core). In the MR space, the seven valence electrons should describe the dominant configuration $3s^2 3p^5$, but they are also free to reorganize themselves in the $n=3$ and $n=4$ subshells with only one occupation constraint: a minimum of five electrons should be either $3s$, or $3p$, as explicitly stated through the notation $\{3s,3p\}^5$. But even with a closed core $\{1,2\}^{10}$, the computational effort is gigantic. Introducing the $\lceil n_{\rm max} l_{\rm max} \rceil$ notation for the orbital active set, the size of the expansion generated with six correlation layers (MR-SD$\lceil 9k \rceil$) reaches 1 895 416 CSF's. Moreover, such a strategy is not efficient, a large number of components being negligible. An interesting approach uses the "multireference interacting" (MR-I) CSF-space defined as the union of the original set of CSF's that belong to the MR, and all CSF's that directly interact with at least one component of the MR, that is,

$$\begin{aligned} &\Phi_i(\gamma_i\ LS) \in {\rm MR\text{-}I} \\ &\quad \Leftrightarrow \exists \Phi_k \in {\rm MR} \quad \text{with} \quad \langle \Phi_i(\gamma_i\ LS)|H|\Phi_k(\gamma_k\ LS)\rangle \neq 0, \end{aligned} \tag{15}$$

for any one-electron radial function basis set $\{P_{nl}(r)\}$. This selection constraint depends on the coupling ordering of the subshells. The conventional coupling hierarchy is a sequential one corresponding to the coupling of each subshell angular momenta to the previous intermediate coupling angular momenta, from left to right [40], for the natural subshell ordering (n and l increasing). But this is not always the most efficient representation. It is indeed common knowledge that the most strongly interacting momenta should be coupled first to get the best physical picture of the resulting levels pattern.

On this basis, we use the *reverse* order of orbitals, coupling sequentially the subshells by decreasing n and l.

Like the MR-SD space, the MR-I configuration set includes at most double excitations with respect to the reference, but the building rule (15) reduces drastically the size of the expansions in comparison with the MR-SD sets. For example, the list of 1 895 416 CSF's discussed previously is reduced to 525 111 CSF's in the MR-I$\lceil 9k \rceil$ model. The corresponding *configuration* reduction is much smaller (18 576 $\rightarrow$ 13 973) since this reduction only arises from the intermediate coupling constraints associated with (15) and not from additional orbital occupation number selection rules. From a practical point of view, the MR-SD expansions are reduced according to the building rule (15) to produce the desired MR-I lists using the LSREDUCE code integrated in the ATSP2K package [35].

Similar to (14), we explore the MR set

$$\mathrm{MR1(S)} = \{1, 2\}^{10}\{3s, 3p\}^{4}\{3\}^{2}, \tag{16}$$

for S. To discuss the delicate balance between the negative ion and the neutral atom, we introduce for the latter a second model, more correlated, based on the following MR set

$$\mathrm{MR2(S)} = \{1, 2\}^{10}\{3s, 3p\}^{4}\{3\}^{1}\{3, 4\}^{1}. \tag{17}$$

The orbital active sets are extended up to $n = 9$, limited to $l \leqslant 7$ (i.e., k orbitals). We use multireference sets with at most two excitations in the $3d$ subshell. Allowing more than one $3d$ electron is indeed necessary for all important intermediate couplings to appear in the set of CSF's satisfying (15).

The MR set (14) contains 157 CSF's. Some sublists of this complete configuration space are selected according to their impact on the energy, mass polarization, and density at the nucleus and used to check the consistency of our results. By investigating the impact of a seventh correlation layer ($10k$) using multireference subsets for S^-, this extra layer is estimated to contribute less than 5×10^{-5} E_h to both ${}^eA$ and $\frac{\hbar^2}{m_e}\Delta S_{\mathrm{SMS}}$.

With the valence correlation expansions based on MR's (14), (16), and (17), we choose to vary all orbitals in the MCHF approach, the frozen-core approximation being considered *a priori* artificial. The mean radii of the spectroscopic orbitals of S and S^- are reported in Table I and compared with the HF ones. As expected, we observe an overall stability of the $n = 2$ orbitals and a larger variation for the ($n = 3$) valence shells, while the $1s$ orbital remains very similar in all calculations. Even if the ($1s^2 2s^2 2p^6$) core is kept closed in the MCHF expansions, some correlation orbitals extend into the inner region of the atom to improve the description of the total wave function. In the sulfur MR2-I$\lceil 9k \rceil$ calculation, for example, the MCHF optimization involves 39 numerical correlation orbitals from which the resulting $6p$, $7d$, $8s$, and $9f$ functions can be qualified as "inner" orbitals by looking at their mean radius ($\langle r \rangle_{nl} < a_0$). Although they still describe the (inner region) valence correlation, they lie in the correct region for estimating core-valence correlation effects through configuration-interaction, as presented in the next section.

TABLE I. Mean radius of spectroscopic orbitals in atomic units of length (units of a_0) obtained for S^- and S with MR1 and MR2 including six correlation layers ($9k$).

	S $3p^4\ {}^3P$			S^- $3p^5\ {}^2P^o$	
nl	HF	MR1-I $\lceil 9k \rceil$	MR2-I $\lceil 9k \rceil$	HF	MR-I $\lceil 9k \rceil$
$1s$	0.097 15	0.097 15	0.097 15	0.097 15	0.097 15
$2s$	0.475 77	0.472 45	0.472 48	0.475 85	0.472 76
$2p$	0.441 04	0.440 61	0.440 61	0.441 06	0.440 37
$3s$	1.720 72	1.714 39	1.610 71	1.776 72	1.778 63
$3p$	2.060 72	2.029 42	1.845 93	2.323 69	2.253 55

2. *Open-core configuration-interaction calculations*

We add to the valence configuration lists, core-valence mono- and multireference SD expansions (MR-CV-SD) created by allowing at most one hole in the core but keeping the $1s$ shell closed and inactive. Core-valence excitations generate much larger lists of configurations than equivalent valence expansions.

For keeping the size of the expansions tractable we use the following procedure. First we sort the configurations of the original MR-I valence eigenvectors into decreasing order by their configuration weights. The latter is defined as the weighted contribution of the CSF's belonging to it

$$w = \sqrt{\sum_{\Phi_i \in \{\mathrm{config}\}} c_i^2}, \tag{18}$$

and are reported in Table II, for S^- and for the two valence models (MR1 and MR2) used for S. Following this hierarchy, we define p reference subsets MR_p containing the first p configurations in the sorted list. Second, we build the corresponding MR_p-CV-SD spaces and keep only the CSF's interacting directly with the complete MR. We denote unambiguously the open-core CI calculations—all performed with six correlation layers—MR-I/CVp.

Table III reports the electron affinity theoretical values calculated with the MR (S^-) and MR2 (S) models. The largest configuration-interaction calculation remains feasible for sulfur (MR2-I/CV15), but the computational limits are definitely exceeded in the negative ion (MR-I/CV31). For S^- indeed, a larger calculation than MR-I/CV14 requires truncating the expansions [41]. To construct the MR-I/CVp spaces for $p = 20$ and $p = 31$, we first omit the CSF's with a $|c_i| < 1.10^{-6}$ in the preceding expansions ($p = 14$ and 20), with an impact smaller than 10^{-6} E_h on both energy and $\frac{\hbar^2}{m_e}\Delta S_{\mathrm{SMS}}$. These lists are then completed by adding the CV expansions of configurations 15–20, and 21–31, respectively.

Table III displays smooth convergence trends along its diagonal, but the largest expansions used for both S and S^- definitely underestimate the nonrelativistic experimental electron affinity (${}^eA_{\mathrm{ref}}^{\mathrm{NR}} = 0.077026\ E_h$), indicating that the neutral system is too correlated with respect to the negative ion. We do not report the corresponding table for MR(S^-)/MR1(S) models (having 4 columns instead of 15) that displays a good convergence toward ${}^eA_{\mathrm{ref}}^{\mathrm{NR}}$.

For a given correlation model, the ΔS_{SMS} parameter is calculated with the wave function expansions that bring the

TABLE II. Weights (w) of the configurations composing MR1, MR2 of S and the MR of S^- in the corresponding MR-I$\lceil 9k \rceil$ wave functions. # denotes the configuration index.

S $3p^4\ ^3P$				S^- $3p^5\ ^2P^o$					
MR1-I $\lceil 9k \rceil$		MR2-I $\lceil 9k \rceil$		MR-I $\lceil 9k \rceil$					
Config.	w	Config.	w	#	Config.	w	#	Config.	w
$3s^23p^4$	0.9567	$3s^23p^4$	0.9151	1	$3s^23p^5$	0.9382	16	$3p^53d^2$	0.0296
$3s3p^43d$	0.1605	$3s^23p^34p$	0.2652	2	$3s^23p^33d^2$	0.1773	17	$3s^23p^33d4s$	0.0292
$3s^23p^23d^2$	0.1568	$3s3p^43d$	0.1573	3	$3s^23p^34p^2$	0.1249	18	$3s^23p^34s^2$	0.0291
$3p^43d^2$	0.0498	$3s^23p^23d^2$	0.1508	4	$3s3p^53d$	0.1045	19	$3p^53d4d$	0.0288
		$3s3p^44s$	0.1256	5	$3s^23p^44p$	0.1030	20	$3s^23p^34s4d$	0.0287
		$3s3p^33d4f$	0.0655	6	$3s3p^44s4p$	0.0748	21	$3p^64p$	0.0252
		$3s3p^33d4p$	0.0632	7	$3s^23p^33d4d$	0.0664	22	$3p^54p^2$	0.0239
		$3s^23p^34f$	0.0531	8	$3s3p^43d4f$	0.0647	23	$3p^54d^2$	0.0203
		$3p^43d^2$	0.0492	9	$3s3p^43d4p$	0.0626	24	$3p^54s^2$	0.0200
		$3p^54p$	0.0310	10	$3s3p^44p4d$	0.0599	25	$3s^23p^34p4f$	0.0173
		$3s^23p^23d4d$	0.0247	11	$3s^23p^44f$	0.0537	26	$3p^54f^2$	0.0124
		$3p^43d4s$	0.0142	12	$3s3p^54d$	0.0447	27	$3s3p^54s$	0.0074
		$3s3p^44d$	0.0127	13	$3s^23p^34d^2$	0.0439	28	$3p^53d4s$	0.0021
		$3p^43d4d$	0.0085	14	$3s^23p^34f^2$	0.0401	29	$3p^54s4d$	0.0020
		$3s^23p^23d4s$	0.0030	15	$3s3p^44d4f$	0.0322	30	$3p^54p4f$	0.0018
							31	$3s3p^44s4f$	0.0010

theoretical electron affinity value as close as possible to the ${}^eA^{\rm NR}_{\rm ref}$ reference value. This approach is supported by the strong correlation observed between the total energy and the $S_{\rm SMS}$ parameter, as discussed in the following. When adding configurations, one by one, in the MR_p of neutral S, we look for the corresponding model in S^- that gives the best energy balance. These values are underlined in Table III and only appear in the first three columns corresponding to MR2-I/CVp ($p = 1 - 3$), all larger $p \geqslant 4$ values underestimating the electron affinity, even for the largest MR-I/CV31 S^- calculation. The three associated S^- correlation models correspond to MR-I/CV1 (mono-reference), MR-I/CV6 and MR-I/CV31, respectively. For the approach based on the less correlated model for S (MR1), we select, using the same criteria, the calculations MR-I/CV4, MR-I/CV6, MR-I/CV12, and MR-I/CV31 of S^- for the four MR1-I/CVp ($p = 1 - 4$) of S, respectively.

3. *Valence and core-valence results*

Table IV reports in two blocks the electron affinities and $S_{\rm SMS}$ differences for the valence correlation models and for their open-core extensions, using the sulfur MR1 and MR2 models, respectively. In the upper half of Table IV, we compare the results of the valence correlation calculations using the MR1-I$\lceil 9k \rceil$ model (see Sec. III D1), with the values obtained from the four CI calculations based on the core-excited correlation models. In the MR(p, p') adopted notation, p refers to the model used for S while p' refers to S^-. According to our approach, the theoretical electron affinity values are forced to

TABLE III. Electron affinity (${}^eA$, in units of $\mathrm{E_h}$) versus the number of configurations (p, p') in $\mathrm{MR2}_p$ for S and $\mathrm{MR}_{p'}$ for S^-. The absolute energy and total number of CSF's (NCSF) of each model MR-I/CVp is given in the first lines and columns of the table. The configurations are taken in the order of increasing weight (see Table II). Underlined are the values of ${}^eA$ in reasonable agreement with ${}^eA^{\rm NR}_{\rm ref} = 0.077026\ \mathrm{E_h}$.

$p'\backslash p$		S	1	2	3	4	⋯	15
	NCSF		235 971	355 354	537 163	681 582	⋯	2 407 805
S^-		E(in $\mathrm{E_h}$)	−397.718 278	−397.722 125	−397.723 707	−397.724 631	⋯	−397.726 165
1	541 780	−397.794 996	<u>0.076 718</u>	0.072 871	0.071 289	0.070 366	⋯	0.068 832
3	864 954	−397.797 229	0.078 951	0.075 104	0.073 522	0.072 598	⋯	0.071 064
4	982 233	−397.797 780	0.079 501	0.075 654	0.074 073	0.073 149	⋯	0.071 615
5	1 088 076	−397.798 944	0.080 666	0.076 819	0.075 237	0.074 313	⋯	0.072 779
6	1 210 344	−397.799 173	0.080 895	<u>0.077 048</u>	0.075 466	0.074 542	⋯	0.073 008
10	2 623 506	−397.799 929	0.081 651	0.077 804	0.076 222	0.075 298	⋯	0.073 764
12	2 854 430	−397.800 229	0.081 951	0.078 104	0.076 522	0.075 598	⋯	0.074 064
14	3 175 092	−397.800 372	0.082 094	0.078 247	0.076 665	0.075 741	⋯	0.074 207
20[a]	3 839 474	−397.800 532	0.082 254	0.078 407	0.076 825	0.075 901	⋯	0.074 367
31[a]	4 339 910	−397.800 667	0.082 389	0.078 542	<u>0.076 960</u>	0.076 037	⋯	0.074 504

[a]These lists are truncated (see text). The actual CSF numbers are 2 089 778 and 2 058 776 for $p = 20$ and 31, respectively.

TABLE IV. Number of CSF's (NCSF), total energy (E, in units of E_h) and S_{SMS} parameters (in units of a_0^{-2}) for S and S^-. The last two columns report the corresponding electron affinity (^eA, in units of E_h) and ΔS_{SMS} (in units of a_0^{-2}). The two sets of results correspond to the zeroth-order multireferences MR1 and MR2 used for S (see text). For each set, the results from the valence models (MR-I$\lceil 9k \rceil$) and the open-core CI calculations [MR(p, p')] are reported.

	S $3p^4\ ^3P$			S$^-$ $3p^5\ ^2P^o$			Δ(S $-$ S$^-$)	
Model	NCSF	E	S_{SMS}	NCSF	E	S_{SMS}	^eA	ΔS_{SMS}
MR1-I$\lceil 9k \rceil$	43 276	−397.673 394	−67.017 49	525 111	−397.751 017	−67.106 00	0.077 62	0.088 5
MR1(1,4)	66 280	−397.720 746	−66.647 70	982 233	−397.797 780	−66.731 63	0.077 03	0.083 9
MR1(2,6)	181 851	−397.722 224	−66.615 36	1 210 344	−397.799 173	−66.711 28	0.076 95	0.095 9
MR1(3,12)	268 647	−397.723 184	−66.603 45	2 854 430	−397.800 229	−66.695 88	0.077 05	0.092 4
MR1(4,31)	408 152	−397.723 563	−66.591 50	4 339 910	−397.800 667	−66.693 35	0.077 10	0.101 8
MR2-I$\lceil 9k \rceil$	209 553	−397.674 938	−67.018 97	525 111	−397.751 017	−67.106 00	0.076 08	0.087 0
MR2(1,1)	235 971	−397.718 278	−66.689 18	541 780	−397.794 996	−66.785 70	0.076 72	0.096 5
MR2(2,6)	355 354	−397.722 125	−66.652 12	1 210 344	−397.799 173	−66.711 28	0.077 05	0.059 2
MR2(3,31)	537 163	−397.723 707	−66.611 43	4 339 910	−397.800 667	−66.693 35	0.076 96	0.081 9
MR2(4,31)	681 582	−397.724 631	−66.597 15				0.076 04	0.096 2
MR2(15,31)	2 407 805	−397.726 165	−66.583 03				0.074 50	0.110 3
NR expt.[a]							0.077 03	

[a]Nonrelativistic electron affinity $^eA^{NR}_{ref}$ defined in Sec. III C.

align with the nonrelativistic experimental value through the (p, p') selection, but there is no such constraint on ΔS_{SMS}. Opening the core through the added CV expansion affects the ΔS_{SMS} by up to 12%. Since the MR1(4,31) calculation corresponds to the complete models, the extracted ΔS_{SMS} is *a priori* reliable. We observed that the results are well aligned, for each system, when plotted in a total energy versus S_{SMS} diagram. Furthermore, the relation is similar for S and S^-. A close analysis of the convergence patterns of the MR1(p, p') results leads to a 10% uncertainty estimation on the calculated ΔS_{SMS}.

The second half of Table IV displays the corresponding results using MR2 for sulfur. A good consistency with the MR1 ΔS_{SMS} values is found for the valence and first open-core [MR2(1,1)] models, but the two larger core-excited CI calculations MR2(2,6) and MR2(3,31) bring unfortunate variations. The effect of the truncation at $p = 3$ of the sulfur MR2-I/CV15 model is estimated by the MR2(4,31) configuration-interaction calculation that slightly underestimates the NR electron affinity. One observes that this extension affects the ΔS_{SMS} value by more than 15%. Furthermore, the complete calculation MR2(15,31) is unreliable, given its large underestimation of $^eA^{NR}_{ref}$.

From all these observations, we reject the open-core CI models based on MR2. Indeed, the sulfur model includes much more correlation than the one built for S$^-$. If one goes from a complete model [MR2(15,31)] that strongly underestimates ^eA to a balanced model that adjusts the electron affinity, it must be through a too-large truncation of the S expansions. The problem of underestimating the S$^-$ correlation energy with respect to the neutral atom's one is then transferred onto another problem, which is the lack of convergence for the latter system (S).

The breakdown of the proposed open-core procedure using the MR2 model for S is probably due to the different nature of the total wave functions obtained for S$^-$ and S. The MR1 approach produces more comparable wave functions for sulfur and its negative ion, respecting the needed balance. Signs for a large difference between the MR1 and MR2 sulfur wave function appear in the analysis of their representation, through the comparison of their respective spectroscopic orbital mean radii (see Table I) and of their configuration weights (see Table II).

E. Theoretical fine structures

The fine-structure splittings are estimated by performing Breit-Pauli configuration-interaction calculations, including the orbit-orbit interaction. The results are presented in Table V. At the Hartree-Fock level of approximation, a large discrepancy between theory and observation ($\simeq$30 cm^{-1}) is found for $^2P^o_{1/2-3/2}$ of S$^-$ and $^3P_{1-2}$ of S. Exploring various models for building the zeroth-order nonrelativistic wave function, we observe that the inclusion of term-mixing due to LS-breakdown does not improve the fine-structure splittings. Valence correlation is definitely insufficient to get a satisfactory agreement, as reflected by the splittings reported in [42]. A "simple" correlation model—denoted SD in Table V—based on single and double excitations up to $6g$ from a single configuration and allowing at most one hole in the $2p$ subshell (i.e., keeping $1s$ and $2s$ closed), improves significantly the agreement between the theoretical and observed fine-structure splitting values. Unfortunately, this agreement is destroyed

TABLE V. Comparison of Breit-Pauli fine-structure splittings (cm^{-1}) with observation.

S$^-$	HF	SD	MR-I/CV31	Observed [3]
$^2P^o_{1/2-3/2}$	−453.03	−482.07	−471.16	−483.54
S	HF	SD	MR1-I/CV4	Observed [3]
$^3P_{1-2}$	−366.91	−394.82	−395.22	−396.06
$^3P_{0-1}$	−181.89	−174.82	−169.93	−177.54

TABLE VI. Experimental and theoretical electron affinity, total isotope shift (IS) and residual isotope shifts (RIS). For the *ab initio* calculations, the specific mass shift (SMS), the total mass shift (MS) and the field shift (FS) contributions are reported separately. All values in 10^{-2} cm^{-1}.

	^eA				IS	RIS
			Observation			
Expt.	16 752 98				+0.23(70)	−1.46(70)
NR exp.[a]	16 905 24					
			Theory[b]			
		SMS	MS	FS		
Valence[c]	16 867(169) 10^{+2}	−1.94(2)	−0.25(2)	0.036(6)	−0.22(3)	−1.91(3)
+ core-valence[d]	16 922(21) 10^{+2}	−2.25(23)	−0.56(23)	0.038(7)	−0.53(24)	−2.22(24)

[a]Nonrelativistic electron affinity $^eA^{\rm NR}_{\rm ref}$ defined in Sec. III C.
[b]Adopting the experimental NMS.
[c]Averaging the MR1-I⌈9k⌉ and MR2-I⌈9k⌉ results (see text).
[d]Using the MR1(4,31) results of Table IV.

when progressively extending the reference space to our more elaborate correlation model, illustrating the difficulty of getting reliable *ab initio* fine-structure splittings.

IV. ISOTOPE SHIFT IN THE ELECTRON AFFINITY: COMPARISON OBSERVATION-THEORY

The observed and theoretical isotope shifts in the sulfur electron affinity, both determined in the present work, are compared in Table VI. The observed isotope shift (IS) on the electron affinity of sulfur is found to be more probably positive, $^eA(^{34}\mathrm{S}) - {}^eA(^{32}\mathrm{S}) = +0.0023(70)$ cm^{-1}, but the uncertainty implies that it may be either "normal" [$^eA(^{34}\mathrm{S}) > {}^eA(^{32}\mathrm{S})$] or "anomalous" [$^eA(^{34}\mathrm{S}) < {}^eA(^{32}\mathrm{S})$]. The normal mass shift (NMS) is easy to estimate from the first term of Eq. (3), NMS = 0.016898 cm^{-1}, using the observed electron affinity. The experimental value of the residual isotope shift (RIS) is obtained by subtracting the NMS contribution to the total isotope shift [i.e., RIS = −0.0146(70) cm^{-1}].

As far as theory is concerned, two sets of results are reported, omitting or including the core-valence excitations, as described in Sec. III D3. For each set, the electron affinity, the specific mass shift (SMS), the total mass shift (MS = NMS + SMS), the field shift (FS), the total isotope shift (IS = MS + FS), and the residual isotope shift (RIS = IS − NMS) are reported. The electron affinities are compared with the experimental nonrelativistic electron affinity ($^eA^{\rm NR}_{\rm ref}$) estimated as explained in Sec. III C, and reported in the same table. The field shift is estimated from Eq. (6) by calculating the change in the electronic densities at the nucleus $\Delta\rho(\mathbf{0})_{\rm NR}$ with the DENSITY program [30]. The error bars of the FS values arise from the uncertainty in the root mean squares of the nuclear charge distributions, converted in a 17% variation of $\delta\langle r^2\rangle^{AA'}$.

For the valence calculations, convergence with respect to the number of correlation layers is achieved in both MR1 and MR2 correlation models. The results reported in the "valence" line are obtained by averaging the MR1-I⌈9k⌉ and MR2-I⌈9k⌉ electron affinities and $\Delta S_{\rm SMS}$ parameters reported in Table IV. Their uncertainty is estimated as half the difference between the two averaged values. The theoretical residual isotope shift [RIS = −0.0191(3) cm^{-1}] compares satisfactorily with the experimental residual isotope shift value (IS − NMS) = −0.0146(70) cm^{-1}.

Opening the core is a very difficult task in the MCHF procedure. The presented open-core CI results are limited to the MR1-based models, due to the breakdown of MR2. The 0.12% and 10% error bars reported on the electron affinity and the SMS values, respectively, are estimated from the convergence of the MR1(p, p') sequence of results (see Table IV). The resulting calculated residual isotope shift of −0.0222(24) cm^{-1}, remains compatible with the experimental RIS and its error bars, but the theory-observation agreement is tenuous. Core excitations affect the SMS contribution by 15%, increasing the total isotope shift by a large factor (2.4). The field shift constitutes a small fraction (∼2%) of the residual shift (SMS + FS) but constitutes an important contribution to the total isotope shift (IS).

Both theory and experiment agree with a strong cancellation between the specific mass shift (SMS) and the normal mass shift (NMS) contributions. Although the normal or anomalous character of the isotope shift in the sulfur electron affinity cannot be strictly confirmed from the present work, the *ab initio* calculations are definitely in favor of an anomalous IS. One should keep in mind, however, that the theoretical error bars are estimated from an objective analysis of the correlation models but do not take into account core-correlation and relativistic effects that are systematically neglected.

ACKNOWLEDGMENTS

T. C. acknowledges support from the "Fonds pour la formation à la Recherche dans l'Industrie et dans l'Agriculture" of Belgium. T. C. and M. G. thank the Communauté française of Belgium (Action de Recherche Concertée) and the Belgian National Fund for Scientific Research (FRFC/IISN Convention) for financial support. They are grateful to Georges Destrée of the ULB-VUB Computing Centre for his help in adapting ATSP2K on the HYDRA cluster.

[1] C. Blondel, C. Delsart, and F. Dulieu, Phys. Rev. Lett. **77**, 3755 (1996).
[2] C. Blondel, C. Delsart, F. Dulieu, and C. Valli, Eur. Phys. J. D **5**, 207 (1999).
[3] C. Blondel, W. Chaibi, C. Delsart, and C. Drag, J. Phys. B: At. Mol. Opt. Phys. **39**, 1409 (2006).
[4] R. Trainham, R. M. Jopson, and D. J. Larson, Phys. Rev. A **39**, 3223 (1989).
[5] I. Lindgren, Phys. Scr. T **120**, 15 (2005).
[6] K. Pachucki and J. Komasa, J. Chem. Phys. **125**, 204304 (2006).
[7] E. Clementi, A. McLean, D. Raimondi, and M. Yoshimine, Phys. Rev. **133**, A1274 (1964).
[8] D. Woon and T. Dunning Jr., J. Chem. Phys. **99**, 3730 (1993).
[9] G. Gutsev, P. Jena, and R. Bartlett, Chem. Phys. Lett. **291**, 547 (1998).
[10] G. de Oliveira, J. M. L. Martin, F. de Proft, and P. Geerlings, Phys. Rev. A **60**, 1034 (1999).
[11] J. M. García de la Vega, Phys. Rev. A **51**, 2616 (1995).
[12] C. Guo-xin, P. Ong, and L. Ting, Chem. Phys. Lett. **290**, 211 (1998).
[13] H. Tatewaki, S. Yamamoto, H. Moriyama, and Y. Watanabe, Chem. Phys. Lett. **470**, 158 (2009).
[14] J. C. Berengut, V. V. Flambaum, and M. G. Kozlov, J. Phys. B: At. Mol. Opt. Phys. **41**, 235702 (2008).
[15] S. G. Porsev, M. G. Kozlov, and D. Reimers, Phys. Rev. A **79**, 032519 (2009).
[16] U. Berzinsh, M. Gustafsson, D. Hanstorp, A. Klinkmüller, U. Ljungblad, and A.-M. Mårtensson-Pendrill, Phys. Rev. A **51**, 231 (1995).
[17] C. Valli, C. Blondel, and C. Delsart, Phys. Rev. A **59**, 3809 (1999).
[18] M. R. Godefroid and C. Froese Fischer, Phys. Rev. A **60**, R2637 (1999).
[19] C. Blondel, C. Delsart, C. Valli, S. Yiou, M. R. Godefroid, and S. Van Eck, Phys. Rev. A **64**, 052504 (2001).
[20] M. Nemouchi, A. Taleb, and M. R. Godefroid, J. Phys. B: At. Mol. Opt. Phys. **37**, 865 (2004).
[21] Isotopic abundances are available online at http://physics.nist.gov/PhysRefData/Compositions /index.html.
[22] C. Blondel, W. Chaibi, C. Delsart, C. Drag, F. Goldfarb, and S. Kröger, Eur. Phys. J. D **33**, 335 (2005).
[23] The identification of commercial products in this paper does not imply a recommendation or endorsement by the National Institute of Standards and Technology, nor does it imply that the items identified are necessarily the best for their purpose.
[24] P. Juncar and J. Pinard, Opt. Commun. **14**, 438 (1975).
[25] C. Blondel, C. Delsart, and F. Goldfarb, J. Phys. B: At. Mol. Opt. Phys. **34**, L281 (2001); **34**, 2757 (2001).
[26] F. Goldfarb, C. Drag, W. Chaibi, S. Kröger, C. Blondel, and C. Delsart, J. Chem. Phys. **122**, 014308 (2005).
[27] W. Chaibi, C. Blondel, C. Delsart, and C. Drag, Europhys. Lett. **82**, 20005 (2008).
[28] G. Audi, A. Wapstra, and C. Thibault, Nucl. Phys. A **729**, 337 (2003).
[29] The mass-equivalent of the electron binding energy is three orders of magnitude smaller than the electron mass contribution.
[30] A. Borgoo, O. Scharf, G. Gaigalas, and M. R. Godefroid, Comput. Phys. Commun. **181**, 426 (2010).
[31] P. Aufmuth, K. Heilig, and A. Steudel, At. Data Nucl. Data Tables **37**, 455 (1987).
[32] I. Angeli, At. Data Nucl. Data Tables **87**, 185 (2004).
[33] C. Froese Fischer, *The Hartree-Fock Method for Atoms. A numerical approach* (Wiley and Sons, New York, 1977).
[34] C. Froese Fischer, T. Brage, and P. Jönsson, *Computational Atomic Structure - An MCHF Approach* (Institute of Physics Publishing, Bristol, 1997).
[35] C. Froese Fischer, G. Tachiev, G. Gaigalas, and M. Godefroid, Comput. Phys. Commun. **176**, 559 (2007).
[36] M. Godefroid, C. Froese Fischer, and P. Jönsson, Phys. Scr. T **65**, 70 (1996).
[37] P. Jönsson, C. Froese Fischer, and M. Godefroid, J. Phys. B: At. Mol. Opt. Phys. **29**, 2393 (1996).
[38] A. Hibbert, R. Glass, and C. Froese Fischer, Comput. Phys. Commun. **64**, 455 (1991).
[39] L. Sturesson and C. Froese Fischer, Comput. Phys. Commun. **74**, 432 (1993).
[40] U. Fano, Phys. Rev. A **140**, 67 (1965).
[41] To perform this CI calculation (3 175 092 CSFs), we used 24 processors of 2.4 GHz during about 24 hours. The matrix and whole set of useful integrals were stored on disk and took a space of 500 Gb. The memory necessary to run the Davidson algorithm implemented in ATSP2K was 11 Gb/proc. Getting the lowest root from the H matrix took around 22 minutes of CPU time/proc.
[42] C. Froese Fischer, G. Tachiev, and A. Irimia, At. Data Nucl. Data Tables **92**, 607 (2006).